Proceedings of the 21st International Conference on Global Research and Education (Inter-Academia 2024)

ZnSe Window Thin Films as Candidate for Sb_2Se_3 Solar Cells

I. Gadiac[a,*], D. Untila[b], I. Lungu[a], M. Dobromir[c] and T. Potlog[b]

[a]*Doctoral School "Natural Sciences", Moldova State University, 60 Al. Mateevici St., MD-2009, Chişinău, Republic of Moldova*
[b]*Laboratory of Organic/Inorganic Materials for Optoelectronics, Moldova State University, 60 Al. Mateevici St., MD-2009, Chişinău, Republic of Moldova*
[c]*Research Centre on Advanced Materials and Technologies, Department of Exact and Natural Sciences, Institute of Interdisciplinary Research, Alexandru Ioan Cuza University of Iasi, 11 Carol I Blvd., 700506, Iasi, Romania*

Doi: 10.12693/APhysPolA.146.424 *e-mail: gadiac.ivan@usm.md

The influence of the technological conditions on the structure of ZnSe thin films deposited by the close-spaced sublimation method onto SnO_2/glass and ITO/glass substrates was studied. The manufacturing parameters were optimized by varying substrate temperature. The X-ray diffraction analysis of the ZnSe thin films showed that films deposited at both types of substrates were polycrystalline in nature with zinc-blende structure, and a preferential peak corresponded to (400) plane for SnO_2/glass regarding the substrate temperature, while for ITO/glass substrate with increasing substrate temperature, it was changing from (111) to (220). The elemental composition of ZnSe thin films deposited onto SnO_2/glass and ITO/glass substrates was confirmed by the energy-dispersive and X-ray photoelectron spectroscopy techniques. Also, ZnSe/Sb_2Se_3 heterostructures have been fabricated with SnO_2/glass and ITO/glass substrates and investigated for their use in photovoltaic applications. This paper also examined how varying the type of transparent electrode used in solar cell fabrication impacts the device's photovoltaic parameters.

topics: close-spaced sublimation (CSS), X-ray diffraction (XRD), X-ray photoelectron spectroscopy (XPS), J–V characteristics

1. Introduction

A literature analysis reveals that in the past, attempts were made by several scientists, to obtain reproducible ZnSe films for device applications [1–3]. More progress has been achieved in the fabrication of blue light-emitting diodes [4], dielectric mirrors [5], filters, blue laser diodes, and other optically sensitive devices [6–8]. There are a number of reports on the different structural, optical, and electrical properties of ZnSe polycrystalline thin films prepared by various techniques such as chemical vapor deposition [9], *metal–organic chemical vapor deposition* (MOCVD) [10], electrodeposition [11], *chemical bath deposition* (CBD) [12], pulsed laser deposition [13], and thermal evaporation [14]. Because of its large band gap of 2.67 eV, ZnSe has been used as a window layer for the fabrication of solar cells. ZnSe thin film has higher transmittance, which allows incoming light to collide enormously with the p–n junction placed below the window layer. It also has lower reflectance because of its wider bandgap and polycrystalline behavior in the visible and ultraviolet regions. Thus, the incident photon trapping increases the resulting enhancement of the photoelectric effect, causing current density to increase. The use of ZnSe films as a heterojunction partner in II–VI thin-film solar cells has been shown to be promising for solar appliances [15]. The ZnSe/CdTe solar cells grown by close-spaced sublimation have yielded fairly good results, with an efficiency of 4.7% [16]. Parent et al. [17] reported a 4.27% efficiency on the photoassisted *metal–organic vapor-phase epitaxy* (MOPVE) ZnSe/GaAs heterojunction solar cells. The researchers obtained solar cells with V_{oc}, J_{sc}, and fill factor (FF) of 0.411 V, 1.245×10^{-5} A, and 43.3%, respectively. Also, ZnSe/GaAs solar cells were fabricated using *molecular beam epitaxy* (MBE) with an efficiency of 4%. The close-spaced sublimation method is considered one of the most promising techniques

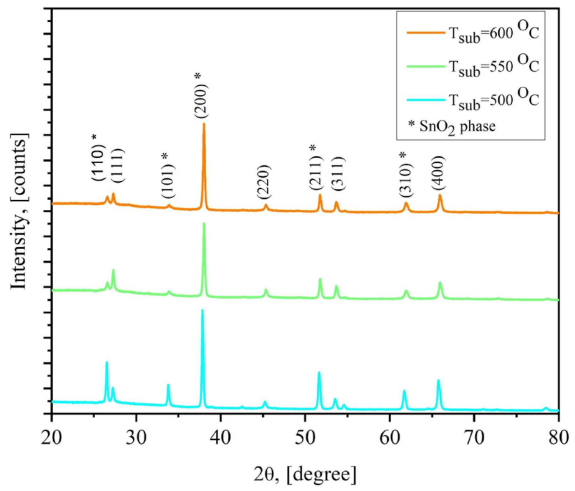

Fig. 1. X-ray diffraction patterns of ZnSe thin films on SnO_2/glass substrates at different substrate temperatures.

for A_2B_6 thin film growth. Therefore, we have used the close-spaced sublimation method (CSS) for the deposition of the ZnSe thin films at different substrate temperatures to prepare SnO_2/ZnSe/Sb_2Se_3 and ITO/ZnSe/Sb_2Se_3 photovoltaic devices. This paper will discuss ZnSe thin films obtained by the CSS technique on ITO/glass and SnO_2/glass substrates.

2. Experimental details

The ZnSe thin films were obtained using a high-vacuum deposition system, specifically the BUП-4 installation, operating at a high vacuum pressure of 1.5×10^{-5} Torr. The deposition process was carried out on ITO/glass substrates, with three substrate temperatures (T_{sub}) maintained: 450, 500, and 550°C. For ZnSe deposited on SnO_2/glass substrates, the substrate temperatures were kept at 500, 550, and 600°C. Throughout the deposition, the source temperature (T_{ev}) was maintained at 700°C to ensure uniform evaporation of the source material. The deposition duration was also kept constant at 3 min to achieve a consistent thickness and quality of the ZnSe films across all samples.

All Sb_2Se_3 thin films were obtained using substrates with ZnSe thin films deposited at an evaporator temperature of 700°C and a substrate temperature of 500°C for 3 min. The set obtained on SnO_2/ZnSe substrates was performed to study absorber layer thickness on photovoltaic parameters (varying parameter was deposition time). Deposition temperatures were 450°C for the substrate and 550°C for the evaporator. Another set obtained on ITO/ZnSe was made with different deposition temperatures and a deposition time of 3 min.

TABLE I

The microstructural parameters of ZnSe thin films deposited on SnO_2/glass substrates.

Samples	Lattice constant		D [nm]	$\varepsilon(\times 10^{-4})$
	a [Å]	c [Å]		
ZnSe_500°C	5.6707	–	28.0	1.0
SnO_2	4.7502	3.1932	63.5	1.5
ZnSe_550°C	5.6572	–	31.7	1.6
SnO_2	4.7365	3.1881	57.9	2.1
ZnSe_600°C	5.6571	–	33.7	2.3
SnO_2	4.7392	3.1871	64.7	2.1

The crystal structure was studied by X-ray diffraction using a Bruker AXS, D8 ADVANCE diffractometer (Cu K_α radiation, 40 mA, 40 kV), with a Ni filter, in the 2θ range of 20°–80°, with a scanning speed of 0.5°/min. The XRD analysis was performed using Rigaku software PDXL. The *energy dispersive spectroscopy* (EDS) analysis of the samples was performed with a JEOL JSM-6390LV scanning electron microscope, operating in high vacuum and low vacuum modes, offering a resolution of up to 3 nm at 30 kV. Information on surface elemental composition and chemical states of the elements present at the sample surface was also derived from theX-ray photoelectron spectroscopy (XPS) measurements carried out using a PHI 5000 VersaProbe photoelectron spectrometer. The XPS spectra were recorded using monochromated Al K_α radiation (1486.7 eV), and the C 1s core level signal was used for calibration of the binding energies in the XPS spectra. The binding energy values were accurate within ±0.2 eV.

3. Results and discussion

The *X-ray diffraction* (XRD) patterns of ZnSe thin films deposited on SnO_2/glass substrate at varying substrate temperatures from 500 to 600°C are shown in Fig. 1. The XRD pattern reveals strong peaks corresponding to the polycrystalline SnO_2 tetragonal crystallographic system, $P42/mnm$ space group, along with some weaker peaks associated with the ZnSe phase. The microstructural parameters of the ZnSe thin films are summarized in Table I. According to them, the ZnSe grains on the SnO_2 substrate are smaller compared to the SnO_2 grains. The change in the lattice constant of ZnSe with different substrate temperatures is not very prominent and suggests that the film grains are stressed. This stress could be due to lattice mismatch and/or differences in the thermal expansion coefficients between SnO_2 and the glass substrate.

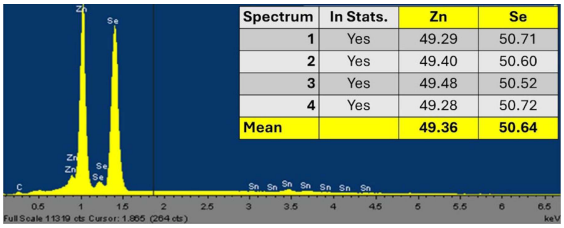

Fig. 2. The EDX analysis of ZnSe thin films deposited on *indium tin oxide* (ITO) substrate.

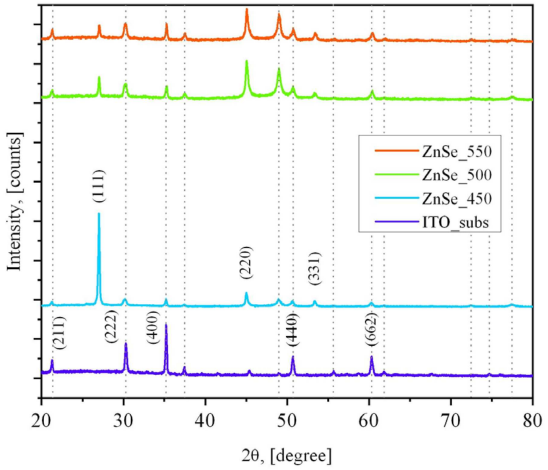

Fig. 3. The XRD patterns of ZnSe thin films deposited at different substrate temperatures on ITO/glass substrate.

The intensities of the (111), (220), and (311) peaks are low in comparison with the (400) one. This indicates a preferential orientation of microcrystallites with the (400) direction. The (400) peak intensity decreases with increasing substrate temperature.

The increase in the strain with increasing substrate temperature indicates the formation of higher quality films at lower substrate temperatures. At the substrate temperature above 500°C, their crystallinity degrades due to the high thermal energy of the adatoms of the ZnSe thin film. This result may be ascribed to low atomic mobility at low substrate temperatures, thereby leading to the formation of a preferred orientation along the (400) plane, which corresponds to the ZnSe phase. At 550°C, the intensity of the (311) plane, which belongs to the $ZnSeO_3$ phase, starts to increase.

Figure 2 presents the *energy dispersive X-ray* (EDX) analysis of ZnSe thin films deposited at a substrate temperature of 600°C. Data for films deposited at other substrate temperatures are not shown, as they exhibit very similar characteristics. The ZnSe films are observed to be Zn-deficient. This deficiency is attributed to the higher vapor pressure of Se compared to Zn and the differing sticking coefficients of the two elements.

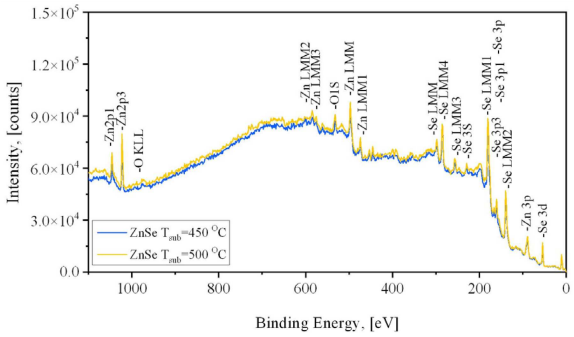

Fig. 4. The XPS survey scan spectra of ZnSe thin films deposited at 450°C and 500°C.

TABLE II

The microstructural parameters of ZnSe thin films deposited on ITO/glass substrates.

T_{sub} [°C]	a [Å]	$d_{[1\,1\,1]}$ [Å]	$I_{[1\,1\,1]}$ [counts]	D [nm]	ε ($\times 10^{-3}$)
450	5.7165	3.3004	4795	280.24	3.24
500	5.7129	3.2984	639	108.70	2.53
550	5.7076	3.2953	465	45.11	0.84

The XRD patterns of ZnSe films deposited on ITO/glass substrate prepared at different T_{sub} are presented in Fig. 3.

Thin films obtained at 450°C exhibit a pronounced orientation along the (111) plane, observed at $2\theta = 27.01°$. As the substrate temperature increases, the growth orientation of ZnSe shifts to the (220) plane. The X-ray diffraction patterns confirm that the ZnSe films are polycrystalline with a cubic structure, which at higher T_{sub} indicates random orientation of crystallites in these films (JCPDS card No. 05-0522). Table II provides microstructural parameters of studied samples.

The average size of the crystallites decreases as the substrate temperature increases, from 280.24 nm at 450°C to 45.11 nm at 550°C. Simultaneously, the lattice constant decreases from 5.7165 to 5.7076 Å with the rise in temperature from 450 to 550°C and is higher than the value observed in films deposited on SnO_2/glass substrates, where it is 5.6572 Å at 550°C. The lattice strain ε also decreases from 3.24×10^{-3} to 0.84×10^{-3}. This reduction in lattice strain with increasing substrate temperature suggests that the film grains are under stress, likely due to changes in the nature and concentration of native defects. Additionally, this decrease may indicate an improvement in the crystallinity of the film.

Figure 4 shows the survey *X-ray photoelectron spectroscopy* (XPS) spectra of ZnSe films obtained at 450 and 500°C, covering the entire binding energy region. The spectra reveal characteristic peaks corresponding to O 1*s*, Se 3*d*, and Zn 2*p* and the chemical composition is presented in Table III.

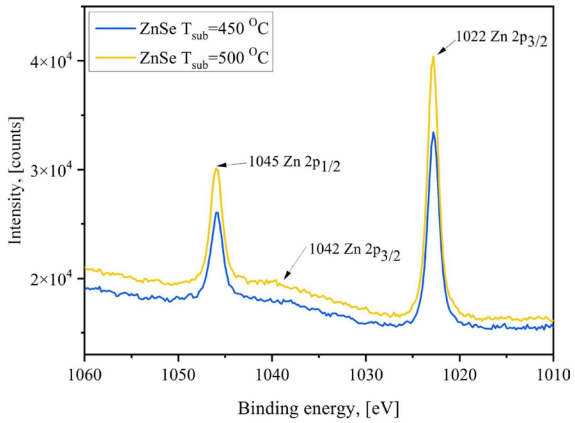

Fig. 5. The XPS spectra of Zn $2p$ thin films deposited at 450°C and 500°C.

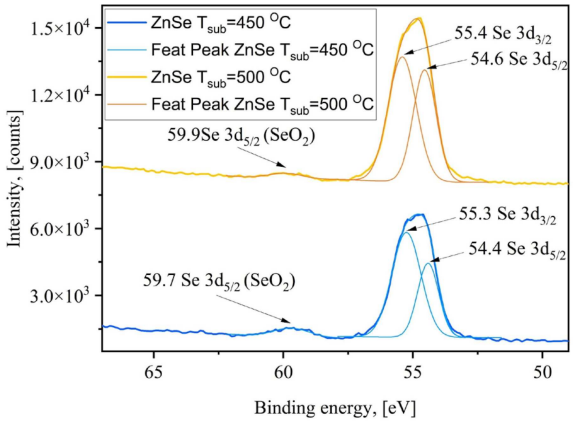

Fig. 6. The XPS spectra of Se $3d$ thin films deposited at 450°C and 500°C.

TABLE III

Chemical composition of ZnSe thin films.

T_{sub} [°C]	Atomic [%]		
	Zn $2p$	O $1s$	Se $3d$
450	35.4	34.3	30.3
500	36.7	33.3	30.0

The C $1s$ core level for the sample deposited at 450°C is located at a binding energy value of 285.3 eV, while for the ZnSe deposited at 500°C, the value shifts to 285.7 eV. These values were used as a reference for correcting the charge shift.

Figure 5 displays the high-resolution Zn $2p_{3/2}$ and Zn $2p_{1/2}$ doublet for ZnSe thin films deposited at 450 and 500°C, which serves as a key indicator of the chemical state of zinc in the material. Deconvolution of these spectra reveals two prominent peaks at 1022 and 1045 eV, as well as a weaker peak around 1042 eV. The main peaks at 1022 and 1045 eV correspond to Zn $2p_{3/2}$ and Zn $2p_{1/2}$ of ZnSe, respectively. The variations in substrate temperature could influence the local state of zinc and selenium, thereby affecting the exact positions of the peaks. The weak bands at 1042.45 eV at 450°C and 1040.87 eV at 500°C may suggest the presence of zinc oxide.

Figure 6 shows the high-resolution Se $3d$ spectra for ZnSe thin films deposited at 450 and 500°C. Deconvolution of these spectra reveals a prominent peak at 54.46 eV for the sample deposited at 450°C and at 54.49 eV for the sample deposited at 500°C, which typically corresponds to Se $3d_{5/3}$ in ZnSe. Also, deconvolution shows that there are peaks at 54.91 eV for 450°C and 55.09 eV for 500°C which correspond to Se $3d_{3/2}$ spectral line which was reported by other researchers [18].

The minor shift in the 55 eV peak position between the two samples may indicate a change in the chemical state of selenium or in the local structure of the material at different substrate temperatures. A weaker peak was observed at 59.77 eV for the 450°C sample and at 59.89 eV for the 500°C sample, suggesting the presence of SeO_2, specifically for the $3d_{5/2}$ line, which is consistent with literature-reported values [19].

Figure 7 shows the high-resolution O $1s$ spectra for ZnSe thin films deposited at 450 and 500°C. Deconvolution of these spectra reveals a prominent peak at 532.1 eV associated with zinc oxide (ZnO), which may form because of the oxidation of ZnSe. The high binding energy component located at 532.52 eV is associated with O^{-2} ions in oxygen-deficient regions within the matrix of ZnO, which are present as inherent deficiency states in the ZnO matrix.

So, composition analysis by XPS shows that films are composed of a mixture of ZnSe, ZnO, and $ZnSeO_3$ phases. Additionally, XPS suggests the presence of oxidized states of selenium, such as SeO_2 or SeO_3.

4. Photovoltaic parameters of ZnSe/Sb_2Se_3 thin-film solar cells

The antimony selenide (Sb_2Se_3) thin films are a promising photovoltaic (PV) absorber with steadily increasing power-conversion efficiency (PCE) compared to other emerging compounds.

According to [20], SCAPS-1D simulation software shows that ZnSe satisfies the fundamental criteria of having good carrier mobility, high electrical conductivity, and an appropriate energy band alignment with minimum conduction band of antimony selenide (Sb_2Se_3).

The photovoltaic characteristics of ZnSe/Sb_2Se_3 thin-film solar cells were investigated using the wide SnO_2 and ITO band gap components at room temperature (300 K) and 100 mW/cm^2 illumination.

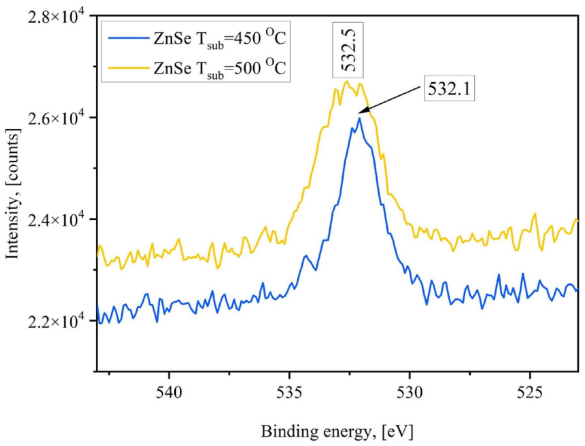

Fig. 7. The XPS spectra of O 1*s* thin films deposited at 450 and 500°C.

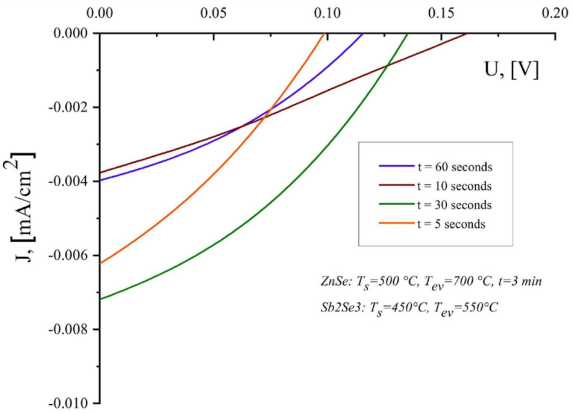

Fig. 8. The *J*–*V* characteristics of SnO_2/ZnSe/Sb_2Se_3/Ag structures for different deposition time of Sb_2Se3.

TABLE IV

The photovoltaic parameters of SnO_2/ZnSe/Sb_2Se_3/Ag structures for different deposition times of ZnSe.

t [s]	V_{oc} [V]	J_{sc} [mA/cm^2]	FF [%]	R_S [kΩ]	R_{Sh} [kΩ]
60	0.11	0.04	34.6	11.4	145.3
10	0.16	0.04	26.7	28.6	55.4
30	0.13	0.07	35.2	9.0	95.5
5	0.09	0.06	34.1	8.8	49.5

The density current–voltage (*J*–*V*) characteristics of SnO_2/ZnSe/Sb_2Se_3/Ag thin-film solar cells are presented in Fig. 8. The photovoltaic parameters of SnO_2/ZnSe/Sb_2Se_3/Ag structures are presented in Table IV.

The density current–voltage (*J*–*V*) characteristics of Sb_2Se_3 solar cells with ZnSe/ITO glass substrates are illustrated in Fig. 9. ZnSe thin

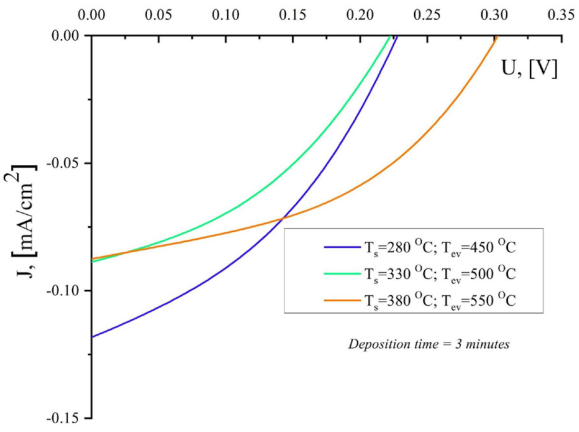

Fig. 9. The *J*–*V* characteristics of ITO/ZnSe/Sb_2Se_3/Ag structures for different technological parameters of Sb_2Se_3.

TABLE V

Photovoltaic parameters of ITO/ZnSe/Sb_2Se_3/Ag structures for different technological parameters of Sb_2Se_3.

T_{sub} [°C]	T_{ev} [°C]	V_{oc} [V]	J_{sc} [mA/cm^2]	FF [%]	R_S [kΩ]	R_{Sh} [kΩ]
280	450	0.23	0.12	37.6	8.4	58.2
330	500	0.22	0.09	39.8	7.2	104.9
380	550	0.30	0.08	44.6	8.3	138.0

films were also obtained at an evaporator temperature of 700°C and substrate temperature of 500°C for 3 min. The deposition time of Sb_2Se_3 layers is 10 min. The photovoltaic parameters of ITO/ZnSe/Sb_2Se_3/Ag structures are presented in Table V.

The highest value of the open-circuit voltage is obtained for ITO/ZnSe/Sb_2Se_3/Ag structures, while the short-circuit current density values are quite modest.

5. Conclusions

In summary, ZnSe thin films were prepared under different growth temperatures on SnO_2/glass and ITO/glass substrates using the CSS method. Performing structural analysis of the samples and calculating *full width at half maximum* (FWHM) values of peaks and the crystalline sizes, we could deduce that for ZnSe deposited on SnO_2/glass, better crystal quality can be achieved at relatively high growth temperatures such as 550°C or 600°C, while for films deposited on ITO/glass at low temperature of 450°C. EDS results revealed that ZnSe films deposited on SnO_2/glass are Zn-deficient, while according to XPS results, the ZnSe films deposited on ITO/glass are composed of a mixture of ZnSe

and ZnO, in which we can clearly see Se deficiency. The peaks observed in XPS measurements suggest the presence of oxidized states of selenium and zinc, such as ZnO, $ZnSeO_3$, SeO_2, or SeO_3. Current–voltage characteristics measured in AM1.5 condition show that ZnSe films are suitable for photovoltaic applications and better voltages can be obtained for ZnSe deposited on ITO/glass substrates. The efficiency and overall performance of solar cells are influenced by various factors, including the incorporation of series resistances (R_S) and shunt resistance (R_{Sh}). The *power conversion efficiency* (PCE) is very modest for both types of solar cells because the values of the series resistance are high. The series resistance arises due to the resistive losses in the conductive elements of the solar cell and causes a drop in the fill factor and efficiency.

References

[1] R. Sharma, Himanshu, S.L. Patel, S. Chander, M.D. Kannan, M.S. Dhaka, *Phys. Lett. A* **384**, 126097 (2020).

[2] C. Mehta, G.S.S. Saini, J. M. Abbas, S.K. Tripathi, *Appl. Surf. Sci.* **256**, 608 (2009).

[3] D. Suthar, G. Chasta, Himanshu, S.L. Patel, S. Chander, M.D. Kannan, M.S. Dhaka, *Mater. Res. Bull.* **132**, 110982 (2020).

[4] Y.H. Won, O. Cho, T. Kim et al., *Nature* **575**, 634 (2019).

[5] E.R. Sharaf, I.S. Yahia, M.I. Mohammed, H.Y. Zahran, E.R. Shaaban, *Phys. B Condensed Matter* **602**, 412595 (2021).

[6] J. Yi, Y. Yu, J. Shang, X. An, B. Tu, G. Feng, S. Zhou, *Opt. Express* **24**, 5102 (2016).

[7] F. Cao, S. Wang, F. Wang, Q. Wu, D. Zhao, X. Yang, *Chemi. Mater.* **30**, 8002 (2018).

[8] M. Gao, H. Yang, H. Shen et al., *Nano Lett.* **21**, 7252 (2021).

[9] S. Sagadevan, I. Das, *Aust. J. Mech. Eng.* **15**, 222 (2017).

[10] S. Kumar, F. Fossard, G. Amiri, J.M. Chauveau, V. Sallet, *Nanomaterials* **12**, 2323 (2022).

[11] R. Kowalik, P. Żabiński, K. Fitzner, *Electrochim. Acta V* **53**, 6184 (2008).

[12] Ho Soonmin, *Am. Chem. Sci. J.* **14**, 1 (2016).

[13] S. Li, L. Wang, D. Gao, Y. Pan, X. Han, *Thin Solid Films* **660**, 405 (2018).

[14] S. Hassanien, K.A. Aly, A.A. Akl, *J. Alloys Compd.* **685**, 733 (2016).

[15] V.S.G. Krishna, S. Bhaskar, M.G. Mahesha, *Cogent Eng.* **11**, 2387260 (2024).

[16] N. Spalatu, D. Serban, T. Potlog, in: *CAS 2011 Proc. 2011 Int. Semiconductor Conf.*, 2011, p. 451.

[17] W. Parent, A. Rodriguez, J.E. Ayers, F.C. Jain, *Solid-State Electron.* **47**, 595 (2003).

[18] R.J. Shallenberger, N. Hellgren, *Surf. Sci. Spectra* **27**, 014020 (2020).

[19] C.D. Wanger, W.M. Riggs, L.E. Davis, J.F. Moulder, G.E. Muilenberg, *Handbook of X-ray Photoelectron Spectroscopy*, Perkin-Elmer Corp., 1979.

[20] R. Kumari, M. Mamta, R. Kumar, Y. Singh, V.N. Singh, *ACS Omega* **8**, 1632 (2023).